Hydrology & Earth
System Sciences

Deriving albedo maps for HAPEX-Sahel from ASAS data using kernel-driven BRDF models

P. Lewis,[1] M. I. Disney,[1] M. J. Barnsley[2] and J.-P. Muller[3]

[1] Remote Sensing Unit, Department of Geography, University College London, 26 Bedford Way, London WC1H 0AP, U.K.
[2] Department of Geography, University of Wales, Swansea, Singleton Park, Swansea SA2 8PP, U.K.
[3] Department of Geomatic Engineering, University College London, Gower Street, London WC1E 6BT, U.K.

Abstract

This paper describes the application and testing of a method for deriving spatial estimates of albedo from multi-angle remote sensing data. Linear kernel-driven models of surface bi-directional reflectance have been inverted against high spatial resolution multi-angular, multi-spectral airborne data of the principal cover types within the HAPEX-Sahel study site in Niger, West Africa. The airborne data are obtained from the NASA Airborne Solid-state Imaging Spectrometer (ASAS) instrument, flown in Niger in September and October 1992. The maps of model parameters produced are used to estimate integrated reflectance properties related to spectral albedo. Broadband albedo has been estimated from this by weighting the spectral albedo for each pixel within the map as a function of the appropriate spectral solar irradiance and proportion of direct and diffuse illumination.

Partial validation of the results was performed by comparing ASAS reflectance and derived directional-hemispherical reflectance with simulations of a millet canopy made with a complex geometric canopy reflectance model, the Botanical Plant Modelling System (BPMS). Both were found to agree well in magnitude. Broadband albedo values derived from the ASAS data were compared with ground-based (point sample) albedo measurements and found to agree extremely well. These results indicate that the linear kernel-driven modelling approach, which is to be used operationally to produce global 16 day, 1 km albedo maps from forthcoming NASA Earth Observing System spaceborne data, is both sound and practical for the estimation of angle-integrated spectral reflectance quantities related to albedo. Results for broadband albedo are dependent on spectral sampling and on obtaining the correct spectral weightings.

Introduction

Earth surface albedo is important in energy budget studies at a wide range of spatial scales. Although point measurements can be made with field instruments, remote sensing offers the only reliable, accurate and spatially- and temporally-comprehensive way to estimate albedo on global or regional scales. Given appropriate atmospheric modelling tools, optical remote sensing instruments can measure the surface reflectance in a particular set of directions and illumination angles dictated by the scanning mechanism of the instrument and the trajectory characteristics of the platform. Estimation of albedo from such data involves integration of the bi-directional reflectance in both the angular and spectral domains. If an accurate estimate is required, a sufficient number of well-placed samples is required in each of these domains along with appropriate models to interpolate and extrapolate the observed reflectance field.

In many ways, the estimation of albedo from such data is straightforward, as the instruments provide sampling of a spectral quantity (radiance, thence directional reflectance) which is directly related to the property of interest. Wanner et al. (1997) describe an algorithm to perform this task, to be used with the Moderate Resolution Imaging Spectrometer (MODIS) (Running et al., 1994) and Multi-angle Imaging SpectroRadiometer (MISR) (Diner et al., 1989, 1991) instruments on board NASA's forthcoming Earth Observing System (EOS) satellites. Application of the algorithm involves inverting (linear) kernel-driven models (Wanner et al., 1995) of the surface spectral Bi-directional Reflectance Distribution Function (BRDF) against a sample set of remotely-sensed observations to derive a set of (spectral) model parameters; these can be used to derive spectral bi-hemispherical reflectance $(\bar{\bar{\rho}}(\lambda))$ and directional-hemispherical reflectance data $(\bar{\rho}(\lambda,\vartheta_s))$—where ϑ_s is the solar zenith angle and λ refers

to wavelength—through multiplication by respective angular integrations of the kernels. These ·data· can subsequently be used to generate estimates of broadband albedo through spectral integration.

The aim of this paper is to use and validate this approach in deriving albedo maps from directional reflectance data obtained by NASA's airborne Advanced Solid-state Array Spectrometer (ASAS) (Irons et al., 1991). The high spatial resolution of the ASAS data allows comparison of the derived albedo values with ground measured data. Both the ASAS data and the ground albedo measurements were collected over a range of representative cover types in Niger, West Africa as part of the HAPEX-Sahel field campaign in September and October 1992 (Prince et al., 1995; Goutorbe et al., 1997). The multi-angle data for each of five sites were co-registered and atmospherically-corrected as described by Barnsley et al. (1997b). After de Colstoun et al. (1996), in performing the atmospheric correction a continental aerosol model was assumed, but the resultant reflectance data tend to be rather sensitive to the aerosol model selected. As a partial validation of the magnitude of the reflectance values derived using this procedure, airborne data over a millet canopy are compared with reflectance data simulated by a detailed 3D canopy reflectance model, the Botanical Plant Modelling System (BPMS) (Lewis, 1996; Lewis and Boissard, 1997).

The ASAS data provide spatial estimates of directional reflectance over the five sites, each about 1.5 km², at a spatial resolution of 2–3 m. Calculation of the ratio of surface-leaving to incoming shortwave fluxes (albedo) involves an angular integral of this information. The angular sampling provided by ASAS is rather limited (up to nine view angles per flightline) and so a model describing the directional reflectance for all viewing and illumination angles is required to perform directional interpolation, extrapolation and then angular integration to derive spectral albedo. The relevance to this task of the kernel-driven models, which will be considered further in this paper, has been demonstrated previously for a range of vegetation canopies and other surfaces (Wanner et al., 1997). The models have a number of attractive properties for the work described in this paper (Lewis, 1995). In particular: (i) they are well-suited to modelling the reflectance of heterogeneous surfaces; (ii) they can be rapidly, robustly and straightforwardly inverted (which is important when considering the number of spatial directional reflectance samples for all of the ASAS datasets processed is around 30×10^6 for each waveband); and (iii) angular integrals of reflectance are achieved rapidly by multiplying the model parameters by angular integrals of the kernels.

Conversion of spectral to broadband estimates of albedo involves integration over the solar spectrum. This is achieved by approximating the integration as a weighted summation over a sample set of wavebands. Validation is attempted by comparing albedo derived from the ASAS data and kernel-driven models with hourly point-sample ground measurements of albedo for different cover types.

ASAS reflectance data

BRDF FROM ASAS DATA

Directional radiance data were recorded by ASAS over five sites in the HAPEX-Sahel area:

1) *East Central Super Site*—fallow (hereafter referred to as ECSS_20);
2) *Southern Super Site*—millet (hereafter referred to as SSS_10);
3) *Southern Super Site*—tiger bush (hereafter referred to as SSS_30);
4) *West Central Super Site*—fallow/millet (hereafter referred to as WCSS_10);
5) *West Central Super Site*—tiger bush (hereafter referred to as WCSS_30)

These have been processed to produce at-ground bi-directional reflectance factors (Barnsley et al., 1997b). ASAS obtains images at 9 separate view zenith angles (−55° aft to 70° forward). Several flight lines were flown over each site, at a variety of view azimuth and solar zenith angles (Barnsley et al., 1997b, p. 754). Although 62 wavebands are recorded by ASAS (420–1037 nm), only four of these have been processed so far (495 nm, 555 nm, 646 nm and 862 nm) and are used in this study. This is partly due to the volume of data produced by the ASAS instrument, and partly because of poor signal-to-noise ratios of data in many of the bands. The bands used here were selected to correspond closely with the MODIS wavebands covered by ASAS.

COMPARISON OF ASAS REFLECTANCES WITH BPMS-MODELLED DATA

The accuracy of determinations of broadband albedo from spectral directional reflectance data using BRDF model parameters is highly dependent on the quality of the source ASAS reflectance data. Factors such as the atmospheric correction process and lack of precision in the accuracy of sensor pointing cause uncertainties in both absolute reflectance values and the associated angular information (viewing and illumination zenith and azimuth angles). Generally, errors in co-registration add additional uncertainty to the model parameters, although the co-registration of these datasets is shown by Barnsley et al. (1997b) to be mostly of sub-pixel accuracy. Due to these other potential sources of error, however, it is desirable to have some point of comparison—ideally with measured ground reflectance data—to give some confidence in the magnitude and shape of the ASAS reflectance data before model inversion is performed. In the absence of suitable ground-level reflectance data for comparison, in this study,

Fig. 1. *Image of millet geometric model used in BPMS simulations (view zenith angle 30°, view azimuth angle 45°, solar zenith angle 35°, solar azimuth 35°).*

at-ground reflectance data were generated using a complex 3D canopy reflectance model, the BPMS.

The BPMS is a complex geometric canopy reflectance model designed to accept plant and terrain geometric data from a wide variety of sources (including 3D dynamic plant models, stereo photogrammetric data, direct manual measurements of leaf position, length etc.) and to construct 3D representations of plants in terms of simple model primitives (triangular facets, spheres, cylinders etc.) (Lewis and Boissard, 1997). A 'field' of such plants can be constructed according to some measured or simulated planting pattern and density. Typically, a limited number of defined plant models is distributed over the field using azimuthally-rotated copies ('clones') according to some probability of occurrence for each defined plant model. The use of 'clones' in this way minimises computer memory requirements and permits the simulation of a field of a crop with a limited sample of measured plants. Accurate radiometric simulations of the canopy can then be carried out using the Advanced Radiometric Ray Tracer (ARARAT), a Monte Carlo ray tracing (MCRT) model within the BPMS (Lewis and Muller, 1992). Both bi-directional reflectance and directional-hemispherical reflectance are simulated by the BPMS.

Detailed manual geometric measurements were made of five mature millet plants in the HAPEX-Sahel Southern Super Site millet area (SSS_10) during September 1992. These data are used within the BPMS to construct 3D models of the millet plants (Fig. 1). The millet canopy is constructed by randomly distributing 'clones' of the five measured plants with a row and plant spacing of 2m (determined from field measurements). Leaf and stem spectral reflectance and transmittance properties are calculated from the PROSPECT leaf scattering model (Jacquemoud and Baret, 1990) using parameters typical of a mature monocotyledon plant. Soil spectral directional reflectance data (van Leeuwen *et al.*, 1997) measured *in situ* during HAPEX-Sahel are used to represent soil reflectance in the model. MCRT simulations were carried out over a range of view zenith angles using an isotropic sky radiance function, at each of the four ASAS wavebands used (495 nm, 555 nm, 646 nm and 862 nm), with the same illumination conditions as those under which the ASAS data were acquired, to give a simulated directional reflectance data set corresponding to the atmospherically-corrected ASAS samples.

Comparisons between the simulations and millet reflectances extracted from a relevant area within the
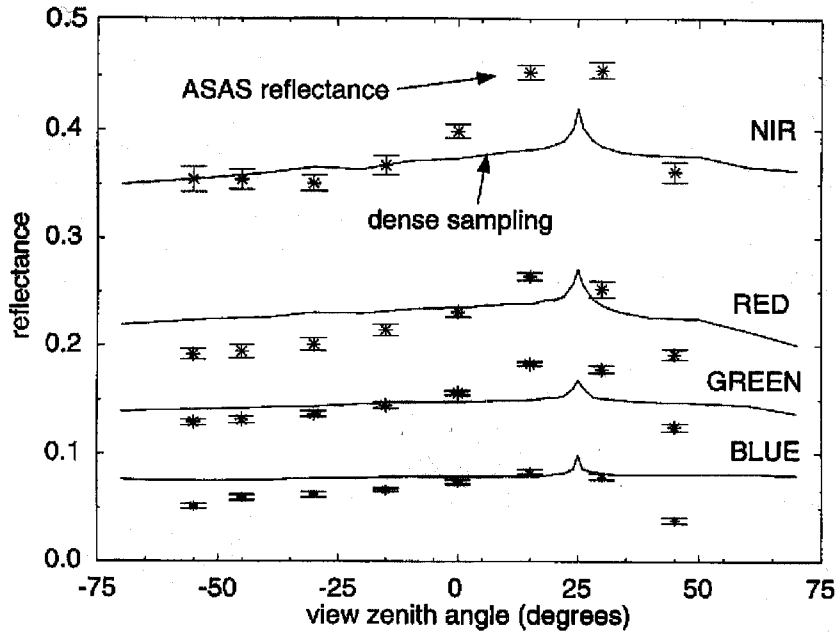
Fig. 2. *Comparison of BPMS-modelled directional hemispherical reflectance with that derived from ASAS using the RossThin and LiSparseModis kernels.*

ASAS data are shown in Fig. 2. The absolute values of the ASAS and BPMS reflectances are of similar magnitude, which gives some confidence in the ASAS reflectance data after radiometric correction using published calibration values and atmospheric correction (Barnsley et al., 1997b). The shapes of the respective BRDFs show similar trends demonstrating a generally downward bowl shape and a retroreflection peak in the 'hot spot' direction (solar zenith angle equal to view zenith angle in the solar principal plane), although the BPMS simulations are slightly flatter than the ASAS data and the ASAS hot spot feature is apparently broader than the BPMS simulation. Lewis and Disney (1997) demonstrate that the majority of directional ('shape') information for such sparse canopies is controlled by the proportion of sunlit soil contributing to the canopy reflectance using an analysis of the same BPMS data. The differences between modelled and measured values may, therefore, be due to irregularities in the real millet data (gaps within the plant stands, variation in planting density etc.). In addition, the shape of the ASAS reflectance is sensitive to the atmospheric aerosol model assumed, which could equally account for the slight discrepancy noted. Whilst it is not clear from this analysis which of these factors might be the cause of the differences here, the overall magnitude and shape of the ASAS reflectance data are generally confirmed for the millet area and hence, for the rest of the ASAS data.

Estimation of spectral albedo from ASAS reflectance data

KERNEL-DRIVEN BRDF MODELS

A kernel-driven model (Roujean et al., 1992) defines the spectral bi-directional reflectance factor, $\rho(\lambda, \vartheta_s, \vartheta_v, \varphi)$—a function of wavelength λ, view zenith angle ϑ_v, solar zenith angle ϑ_s, and relative azimuth angle φ—as:

$$\rho(\lambda, \vartheta_s, \vartheta_v, \varphi) = f_{iso}(\lambda) + f_{vol}(\lambda)k_{vol}(\vartheta_s, \vartheta_v, \varphi)$$
$$+ f_{geo}(\lambda)k_{geo}(\vartheta_s, \vartheta_v, \varphi) \qquad (1)$$

where: f_{iso} is the isotropic parameter (a normalisation term representing the reflectance at nadir with a solar zenith angle of zero); f_{vol} is the volumetric scattering parameter (based on an approximation to single-scattering from a homogeneous volume-scattering medium after Ross (1981)); f_{geo} is the geometric parameter (based on considerations of sunlit and shaded canopy proportions from discrete objects after Li and Strahler (1986)); and k_{vol} and k_{geo} are the kernels associated with the latter two terms. The kernels are, in effect, 'shapes' describing the abstraction of the BRDF given different sets of assumptions about the major scattering processes and a range of simplifications which permit linearisation. The kernels are not orthogonal in the general case (Wanner et al., 1996) and the accuracy of the resultant model parameters will depend on the angular sampling. Typically, the isotropic parameter has the lowest degree of uncertainty, although this depends on the average solar zenith angle of the observations. The expected error in the other terms decreases with increasing kernel variance and decreasing covariance over the

angular sample set. Various sets of approximations can be made in the linearisation stage of model development, for instance assuming the volumetric component to be optically thin (a kernel known as RossThin) or thick (RossThick) (Wanner *et al.*, 1995). The geometric kernels, known generically as Li kernels, involve various approximations and non-linear terms which must be held constant in this process, from which two major kernels, known as LiSparseModis and LiDenseModis (Wanner *et al.*, 1997), may be derived.

BRDF MODEL INVERSIONS AND CALCULATION OF SPECTRAL ALBEDO

Four kernel combinations (isotropic plus RossThick or RossThin and LiSparseModis or LiDenseModis) are inverted against the ASAS reflectance data. The inversion is constrained to keep the model parameters within physically-valid limits—in effect, imposing non-negativity on the model parameters (Lewis, 1995). The choice of which set of kernels is best suited to a particular pixel can be made by using a weighted function of the root-mean-squared error (RMSE) in model inversion (Wanner *et al.*, 1997), although this criterion alone is often insufficient to make a clear decision. Lewis and de Lope (1997) suggest that temporal consistency of RMSE may be a more useful criterion. In the absence of multi-temporal data, spatial consistency over the images is considered as a surrogate. In addition, a particular kernel combination that consistently gives physically realisable (non-negative) parameters over all wavebands is more likely to be appropriate to the surface being modelled. An analysis of these three criteria over all the ASAS data suggests that the most appropriate kernels for these data are isotropic, RossThin (volumetric), and LiSparseModis (geometric). Model parameter information obtained from inversion of these kernels against the reflectance data is shown in Fig. 3. From top to bottom the images show the isotropic, RossThin and LiSparseModis parameter information of the red band (646 nm). Figures 3a to e, respectively, show the parameters for each of the five locations noted above.

Figure 3 suggests that the majority of the reflectance information is contained within the isotropic parameter (the volume-scattering and geometric kernels are normalised to be ≤ 1) and consequently the albedo will be controlled largely by this. The geometric and volume-scattering kernels, the directional components of surface reflectance, contain successively lower magnitude information (and tend to have higher proportionate uncertainties associated with them), but the variation described by these is still significant as the surface reflectance is still distinctly non-Lambertian. This result confirms the findings of Barnsley *et al.* (1997a) on the statistical information content of directional reflectance data over an agricultural area in Lincolnshire in the UK; they concluded that the magnitude of differences in the 'shape' of BRDF over an area

can be significantly less than scene 'brightness variations' (analogous to the volume-scattering/geometric and isotropic parameters respectively). The results shown in Fig. 3 demonstrate the ability of linear BRDF models to extract information on the spatial variability of a parameterisation of directional reflectance, whilst highlighting the difficulty of, accurately characterising the directional component (which may be several orders of magnitude lower than the isotropic component). For the tiger bush sites, the RossThin parameter is close to zero for the bare soil between the shrubs. Similarly, the LiSparseModis parameter is close to zero for the shrub crowns. This supports the Lewis and Disney (1997) analysis of the directional reflectance of millet; the RossThin parameter can indeed model the volumetric scattering within the vegetation and the LiSparseModis parameter can model the shadow variations on the soil background.

Spectral directional-hemispherical reflectance is a function of solar zenith angle. In the kernel-driven modelling approach, this is calculated through:

$$\overline{\rho}(\lambda, \vartheta_s) = f_{iso}(\lambda) + f_{vol}(\lambda)K_{vol}(\vartheta_s) + f_{geo}(\lambda)K_{geo}(\vartheta_s) \quad (2)$$

where K_{vol} and K_{geo} are directional-hemispherical integrals of k_{vol} and k_{geo} respectively (Roujean *et al.*, 1992; Lewis, 1995). The bi-hemispherical integral of reflectance is similarly calculated using bi-hemispherical integrals of the kernels. Note from Eqn. 2 that the kernel integrals can be pre-calculated; the resultant integrated reflectance terms are then simply weighted summations of the model parameters.

Figure 4 compares the spectral directional-hemispherical reflectance of the SSS_10 millet canopy as a function of solar zenith angle calculated from the ASAS data using the kernel-driven model with that simulated directly using the BPMS. The modelling of directional-hemispherical reflectance provided by the BPMS is close to that produced from the kernel-driven models and ASAS data. The discrepancy between the two is carried through from the differences in BRDF shape observed in Fig. 2. The solar zenith angles of the SSS_10 ASAS data ranges from 28° to 46° (Barnsley *et al.*, 1997b). The difference between the two is lower for low solar zenith angles which provides some confidence in the ability of the kernel-driven models and ASAS data to calculate this term from samples over a limited range of sun angles for surfaces such as this. Correct modelling of spectral directional-hemispherical reflectance is more important for energy budget studies at lower solar zenith angles, due to the higher ground-projected irradiance at these angles. The discrepancy between measured and simulated results for the near infrared (862 nm) is poorer than for other wavebands, with the ASAS results apparently over-estimating directional-hemispherical reflectance relative to the BPMS results by around 0.03 at nadir, increasing with increasing solar zenith angle. Generally, however, these results confirm that the ASAS-derived spectral directional-hemispherical
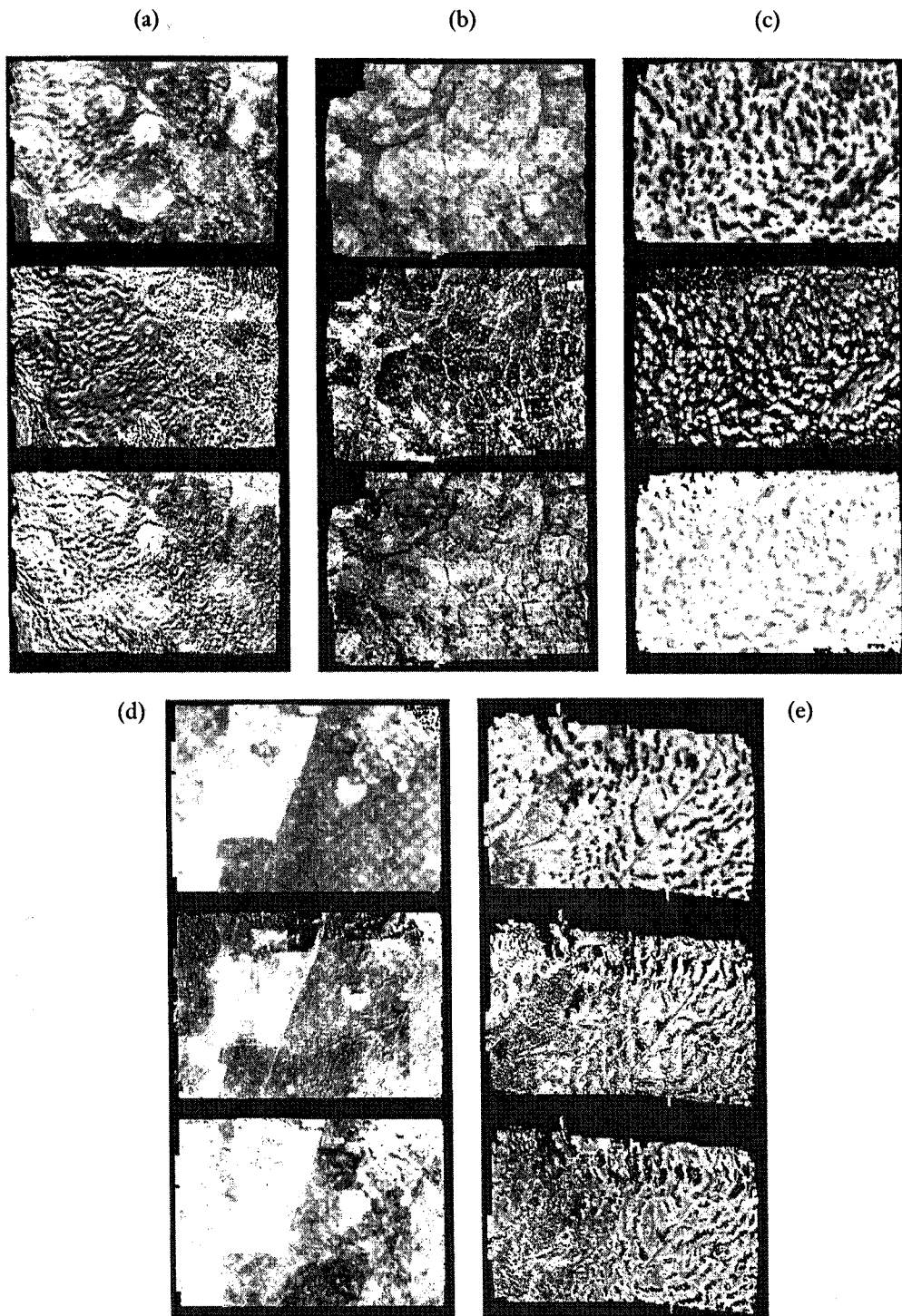
(a)   (b)   (c)

(d)   (e)

Fig. 3. *ASAS-derived BRDF model parameters: Isotropic (scale 0–0.35), RossThin (scale 0–0.025), LiSparseModis (scale 0–0.035) for red band (646 nm) for 5 HAPEX sites:*
  a) East Central Super Site—fallow (ECSS_20)
  b) Southern Super Site—millet (SSS_10)
  c) Southern Super Site—tiger bush (SSS_30)
  d) West Central Super Site—fallow/millet (WCSS_10)
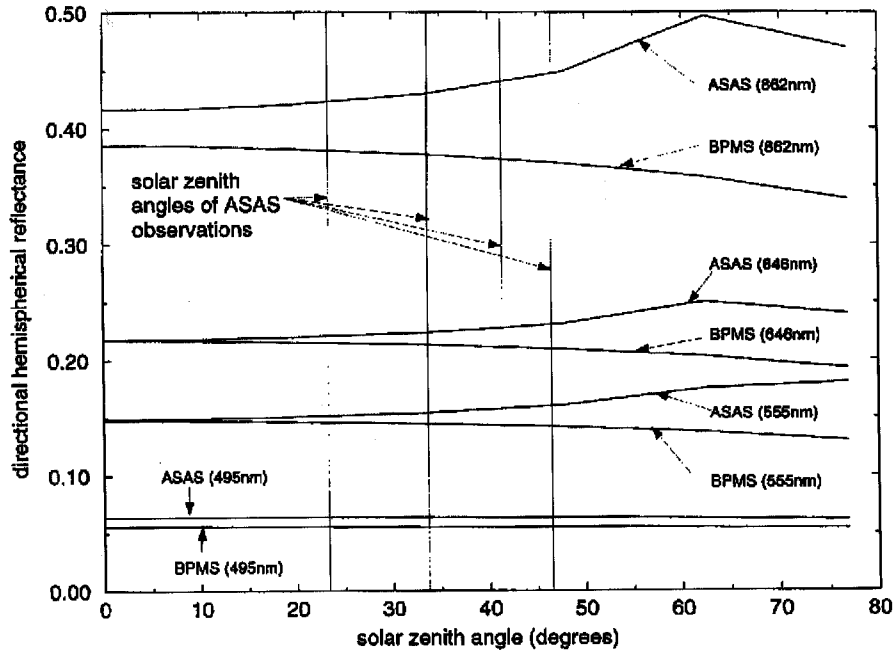 *e) West Central Super Site—tiger bush (WCSS_30)*

Fig. 4. *Directional-hemispherical reflectance of a millet canopy simulated with the BPMS and that produced from the ASAS data and kernel-driven models.*

reflectance for the millet canopy are correct and provide confidence both in the atmospheric correction and the kernel-driven modelling approach used.

Using the information generated from the model inversions, spectral directional-hemispherical reflectance, $\bar{\rho}(\lambda, \vartheta_s)$ (Eqn. 2) and bi-hemispherical reflectance $\bar{\rho}(\lambda)$ are calculated for each waveband. Spectral albedo, $\alpha(\lambda, \vartheta_s)$, can be estimated from these by:

$$\alpha(\lambda, \vartheta_s) = (1 - d(\lambda, \vartheta_s))\bar{\rho}(\lambda, \vartheta_s) + d(\lambda, \vartheta_s)\bar{\rho}(\lambda) \quad (3)$$

where $d(\lambda, \vartheta_s)$ is the proportion of diffuse illumination, a function of wavelength and solar zenith angle. This approximation involves assuming the sky illumination to be isotropic, which is reasonable in the calculation of albedo, other than at high solar zenith angles (Lewis and Barnsley, 1994).

Derivation of broadband albedo

The calculation of broadband albedo $\bar{\alpha}$, from the terms above is given by:

$$\bar{\alpha} = \int_{\lambda 1}^{\lambda 2} W(\lambda, \vartheta_s)\alpha(\lambda, \vartheta_s)d\lambda \quad (4)$$

where $W(\lambda, \vartheta_s)$ is the proportion of total irradiance at that wavelength and solar angle and λ_1 and λ_2 define the wavelength limits of the solar spectrum. More generally, a sample set of wavebands over which to obtain an estimate of the integral is likely to be available. If the wavebands sample the solar spectrum sufficiently well, the integral in Eqn. 4 can be approximated by a weighted summation

over a finite number of wavebands. This approach is adopted here. Information on the direct and diffuse illumination as a function of time (and hence, of solar zenith angle over the range observed at the time of year and location of the data) are calculated using the atmospheric radiation transfer code, 6S (Vermote *et al.*, 1997) with measured atmospheric parameters. Note from Eqn. 4 that, even if the spectral reflectance (hence spectral albedo) is Lambertian, this is not necessarily so for the broadband albedo if W varies as a function of solar zenith angle. Figure 5 shows that the proportional contributions, W, change significantly over the day. For solar zenith angles beyond 70° the information in Fig. 5 may be unreliable as the 6S simulation is not valid (i.e. before 07:14 and after 16:40). Lewis and Barnsley (1994) also note that an isotropic diffuse approximation in the calculations of albedo is poor at low solar elevations.

Figure 6 shows the broadband albedo calculated for the SSS_10 site from the ASAS data and related albedo terms. To obtain sufficient angular samples, data from the 3rd and 9th of September are combined. Figure 6 also shows ground-instrument measured values of broadband albedo for these dates; except at extreme solar zenith angles they give close agreement with the modelled values. It is instructive to examine also ASAS-derived spectral albedo values for the site in the figure, as, from Eqn. 4, the broadband albedo is simply a proportionate weighting of these terms; the broadband albedo must lie between the upper and lower bounds of the spectral albedo data. The wide range which the spectral albedo covers (around 0.05 to 0.45 at solar noon, for example) emphasises the importance
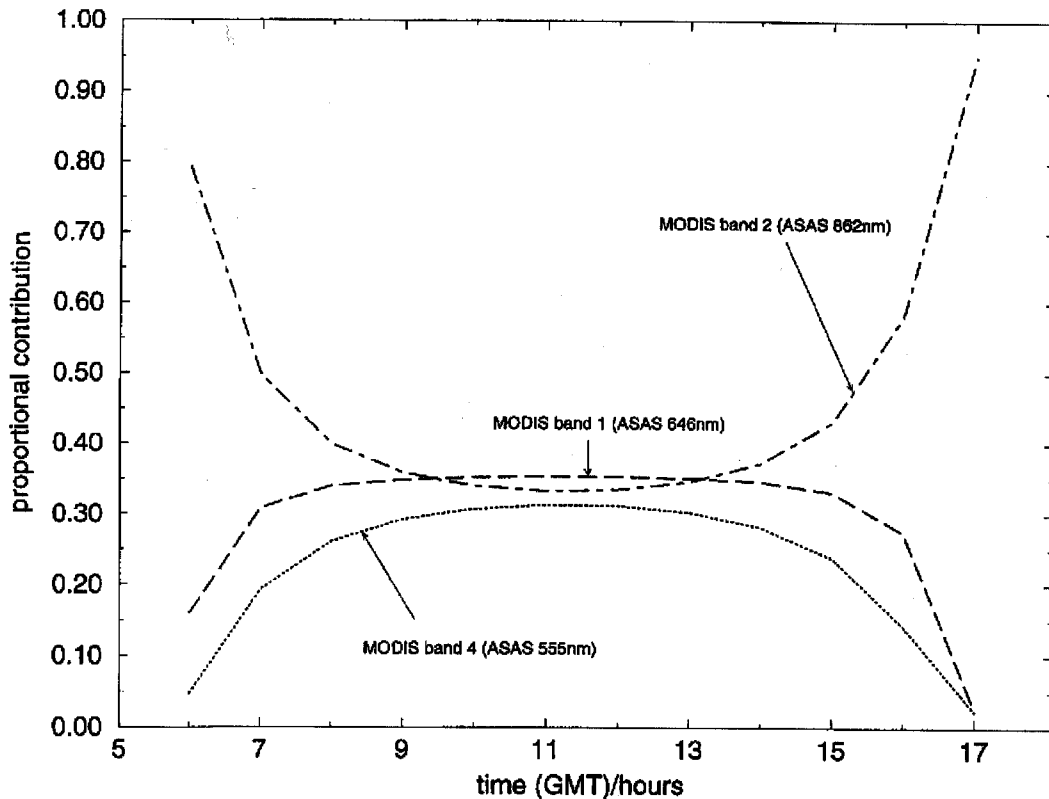
Fig. 5. *Proportion of contribution of solar irradiance per ASAS band throughout the day.*

of correct estimation of the weighting terms. The over-estimation of ASAS-derived albedo at large solar zenith angles seen in Fig. 6 is certainly due to an over-estimation of the near infrared contribution at these angles, though this could arise from an over-estimation of W in Eqn. 4 at these angles and/or an overestimation in near infrared directional-hemispherical reflectance in model extrapolation to these solar zenith angles as suggested by the comparison with the BPMS results (Fig. 4). In any case, a higher error in this region is to be expected, as the assumption in Eqns. 3 and 4 of isotropic diffuse irradiance is poor at high solar zenith angles (Lewis and Barnsley, 1994).

Figure 7 shows similar information to Fig. 6, but for the SSS_30 site. The data are separated into measured and modelled albedo for bare soil and tiger bush shrubs. These data are for a single date (17th September). Again, close agreement is shown, although the soil albedo derived from ASAS appears to be a slight over-estimate; the measured data may be 'contaminated' by some vegetation within the sensor's field of view, which will lower the measured albedo values. It is also worth noting the asymmetry in measured soil albedo at high solar zenith angles, which emphasises the fact that albedo is *not* an intrinsic surface property, but is dependent on the atmospheric conditions at the time of observation. Figure 8 shows a scatterplot of modelled surface radiance calcu-

lated from modelled broadband albedo against measured values for all sites. The high value of the correlation coefficient 0.979, confirms the close agreement between the measured and modelled data. The only noticeable outliers are the values obtained using the ASAS data of only 7 angular samples for SSS_10 for the 3rd September (as opposed to 25 samples for SSS_10 for the 9th September and 19 samples for the SSS_30 site (17th September)); too few samples lead to larger errors in the modelled albedo values. Figure 8, presenting the results as radiance rather than albedo, illustrates that a larger error in estimated albedo is of much less importance at high solar zenith angles, as the solar irradiance at these times of day is so much lower than at either side of solar noon.

Figure 9 shows ASAS derived spatial broadband albedo at 12:00 GMT over all five sites imaged. The areas of very high albedo are bare soil; the areas of low albedo, dense vegetation, such as tiger bush.

Discussion and conclusions

This paper has described the application and testing of a method for deriving spatial estimates of broadband albedo from sparse angular and spectral samples of reflectance available from remote sensing observations. Key stages in processing were seen to be: (i) data pre-processing (accurate image co-registration and atmospheric correction);
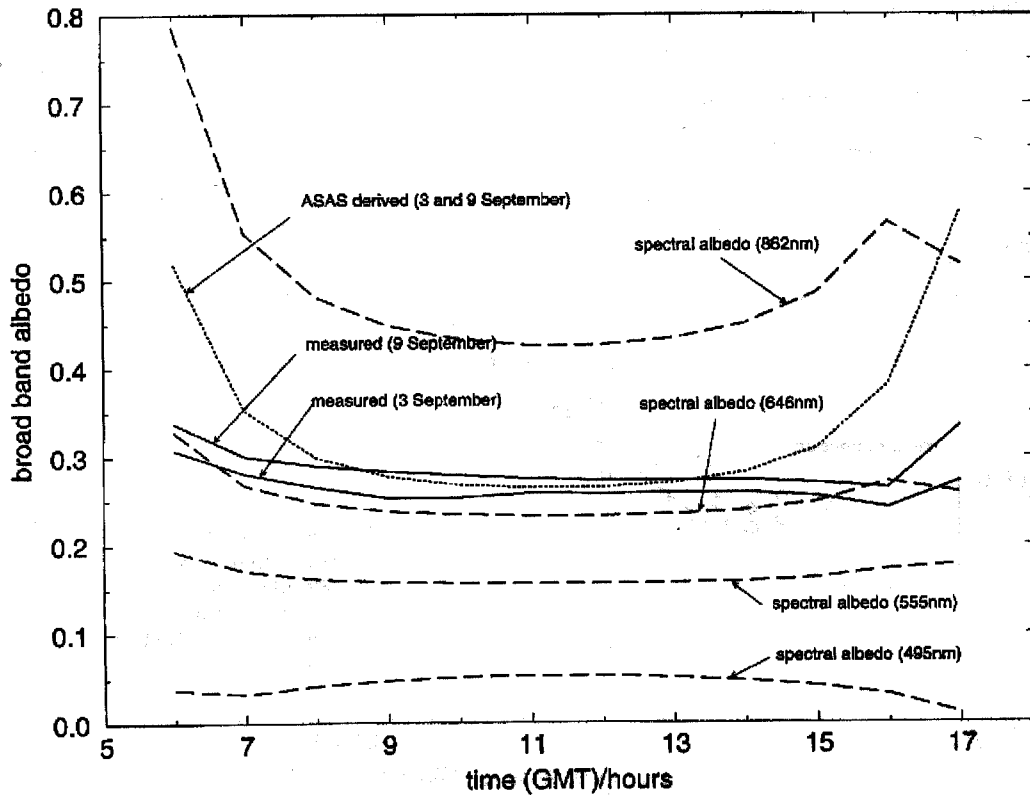
Fig. 6. *Modelled and measured broadband albedo and spectral albedo, Southern Super Site SSS_10 (millet areas).*
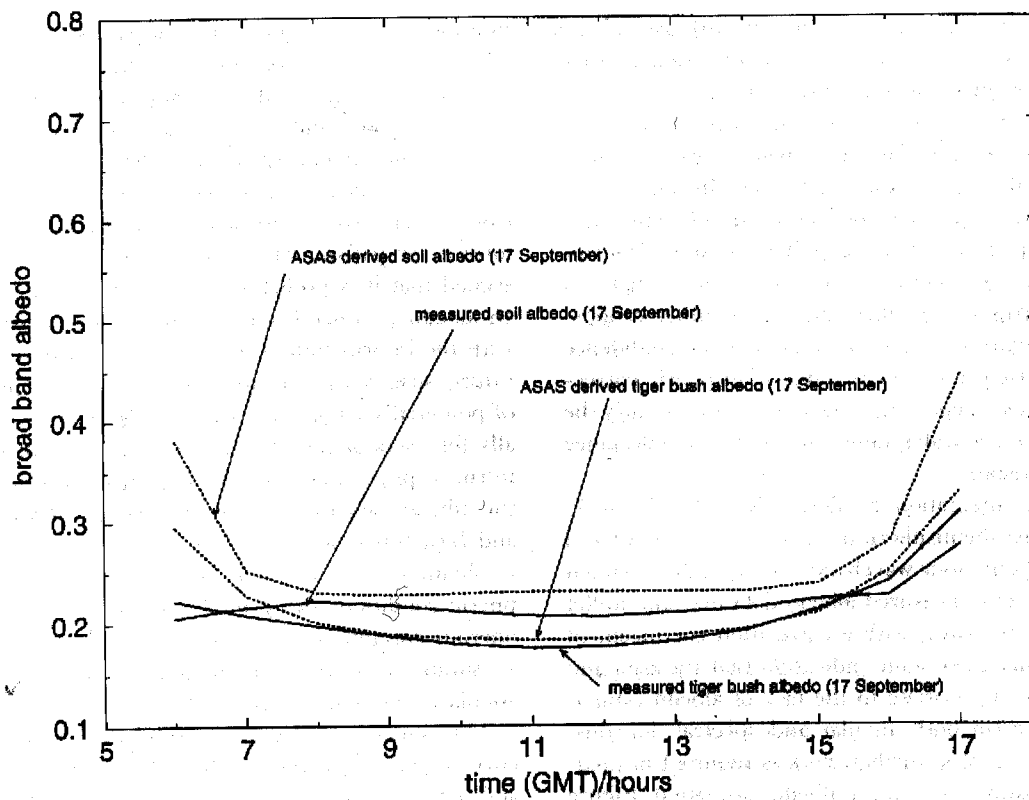

Fig. 7. *Modelled and measured albedo for Southern Super Site SSS_10 (tiger bush and bare soil areas).*
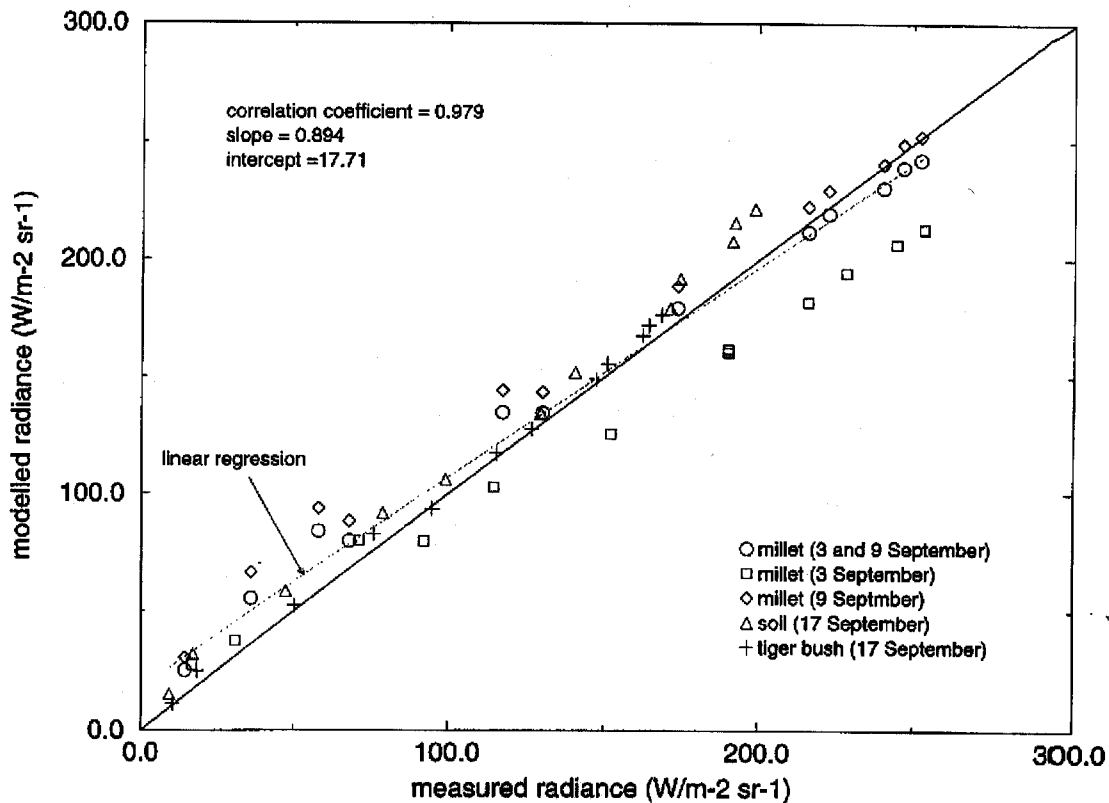
correlation coefficient = 0.979
slope = 0.894
intercept =17.71

linear regression

O millet (3 and 9 September)
□ millet (3 September)
◇ millet (9 Septmber)
△ soil (17 September)
+ tiger bush (17 September)

Fig. 8. *Scatterplot of modelled and measured radiance for all sites.*

(ii) BRDF model selection and fitting; (iii) use of the model parameters to derive spectral directional-hemispherical and bi-hemispherical reflectance; (iv) spectral integration for a given atmospheric state to estimate broadband albedo. An attempt has been made at each stage of processing to validate the results obtained. In the absence of ground-based reflectance data, model simulations using a complex canopy reflectance model have been used to validate, partially, ASAS-derived spectral bi-directional and directional-hemispherical reflectance for a millet canopy. While the results of this analysis provide some confidence in the radiometric pre-processing and atmospheric correction of the ASAS reflectance data, it would clearly be preferable to have a wider range of measured reflectance data for comparison.

The spectral integration to derive broadband albedo from directional-hemispherical and bi-hemispherical reflectance used only four wavebands. The results obtained agree very well with measured albedo data over the millet and soil/tiger bush sites, with a correlation coefficient of 0.979. Whilst this gives some indication that the data and models used are appropriate to the task of albedo estimation from sparse (in both angular and spectral domains) remote sensing samples, further work is required in justifying the waveband selection for albedo estimation. Figure 5 shows how the spectral weighting term, W, can vary sig-

nificantly as a function of time of day (solar zenith angle), and of atmospheric conditions. The diffuse illumination component, $d(\lambda, \vartheta_s)$, will also vary in response to illumination angle and atmospheric variations, once again stressing the fact that albedo is not an intrinsic surface property. Whilst the calculation of remote sensing-derived broadband albedo from these data is indeed necessary to perform a comparison with ground measured data, it can be argued that it is probably not generally useful to produce an albedo product from such data. Although, in dealing with the information derived from the airborne, or in the future, spaceborne sensors, one has to contemplate the use of potentially large datasets, it would be preferable generally for users of the spatial albedo data to incorporate the intrinsic properties, $\bar{p}(\lambda, \vartheta_s)$ and $\bar{p}(\lambda)$ into models using the albedo data rather than $\bar{\alpha}$ directly. Values of $d(\lambda, \vartheta_s)$ and $W(\lambda, \vartheta_s)$ could then be varied within the user's model to obtain an estimate of $\bar{\alpha}$ more appropriate to the atmospheric conditions being modelled. Such a task is not too onerous computationally, since, from Eqns. 2, 3 and 4, $\bar{\alpha}$ is simply a linear combination of the pre-calculated angularly-integrated kernel values.

This paper provides some useful data on the albedo of cover types within the HAPEX-Sahel study site in Niger and demonstrates the application of the kernel-driven modelling approach to this task for high resolution data. In

Acknowledgements

References

Barnsley, M.J., Allison, D. and Lewis, P., 1997a. On the information content of multiple view angle (MVA) images. *Int. J. Remote Sens.*, 18, 1937–1960.

Barnsley, M.J., Lewis, P., Sutherland, M. and Muller, J-P., 1997b. Estimating land surface albedo in the HAPEX-Sahel southern super-site: inversion of two BRDF models against multiple angle ASAS images. *J. Hydrol.*, 188–189, 749–778.

Colstoun, E.C.B. de, Walthall C.L., Cialella, A.T., Vermote, E.R., Halthore, R.N. and Irons, J.R., 1996. Variability of BRDF with land cover type for the west central HAPEX-Sahel super site. *Proceedings of the International Geoscience and Remote Sensing Society Symposium (IGARSS'96)*. IEEE, Pitscataway, NJ, USA., 1904–1907.

Diner, D.J, Bruegge, C.J., Martonchik, J.V., Ackerman, T.P., Davies, R., Gerstl, S.A.W., Gordon, H.R., Sellers, P.J., Clark, J., Daniels, J.A., Danielson, E.D., Duval, V.G., Klassen, K.P., Lilienthal, G.W., Nakamoto, D.I., Pagano, R. and Reilly T.H., 1989. MISR: A Multi-angle Imaging SpectroRadiometer for geophysical and climatological research from EOS. *IEEE Trans. Geosci. Remote Sens.*, 27, 200–214.

Diner, D.J., Bruegge, C.J., Martonchik, J.V., Bothwell, G.W., Danielson, E.D., Ford, V.G., Hovland, L.E., Jones, K.L. and White, M.L., 1991. A Multi-angle Imaging SpectroRadiometer for terrestrial remote sensing from the Earth Observing System. *Int. J. Imaging Sys. and Tech.*, 3, 92–107.

Goutorbe, J-P., Lebel, T., Dolman, A.J., Gash, J.H.C., Kabat, P., Kerr, Y.H., Monteny, B., Prince, S.D., Stricker, J.N.M., Tinga A. and Wallace J.S., 1997 An overview of HAPEX-Sahel: a study in climate and desertification. *J. Hydrol.*, 188–189, 4–17.

Irons, J.R., Ranson, K.J., Williams, D.L., Irish, R.R. and Huegel, F.G., 1991. An off-nadir pointing imaging spectroradiometer for terrestrial ecosystem studies. *IEEE Trans. Geosci. and Remote Sens.*, 29, 66–74.

Jacquemoud, S. and Baret, F., 1990. PROSPECT: a model of leaf optical properties spectra. *Remote Sens. Environ.*, 34:75–92.

Lewis P., 1995. The utility of linear kernel-driven BRDF models in global BRDF and albedo studies, In: *Proceedings of the International Geoscience and Remote Sensing Society Symposium (IGARSS'95)*, July 1995, Firenze, Italy. IEEE, Pitscataway, NJ, USA. 1186–1188.

Lewis P., 1996. A botanical plant modelling system for remote sensing simulation studies, Unpublished PhD., University of London, 349p.

Lewis P. and Barnsley, M.J., 1994. Influence of the sky radiance distribution on various formulations of the earth surface albedo. In: *Proceedings of the 6th International Symposium on Physical Measurements and Spectral Signatures in Remote Sensing* 17–24 January 1994, Val d'Isere, France. ISPRS Commission VII, 707–713.

Lewis P. and Boissard, P., 1997. The use of 3D plant modelling and measurement in remote sensing. In: *Proceedings of the 7th International Symposium on Physical Measurements and Spectral Signatures in Remote Sensing* Courchevel, France. ISPRS Commission VII. Vol. 1., 319–326.

Lewis, P. and Disney, M.I., 1997. Examining BRDF model operation with the botanical plant modelling system, In: *Proceedings of the Remote Sensing Society Annual Conference, Reading, UK*. Remote Sensing Society: Nottingham, 298–303.

Lewis, P. and de Lope, E., 1997. The application of kernel-driven BRDF models and AVHRR data to monitoring land surface dynamics in the Sahel. *Chinese J. Remote Sens. 1 (Special Issue of the First International Workshop on Multiangular Remote Sensing)* 155–161.

Lewis P. and Muller J.-P., 1992. The Advanced Radiometric Ray Tracer ARARAT for plant canopy reflectance simulation, In: *International Archives of Photogrammetry and Remote Sensing: Commission VII*, Washington DC, USA, 29, 26–34.

Li, X. and Strahler, A., 1986. Geometric-Optical Bidirectional Reflectance Modelling of a Conifer Forest Canopy. *IEEE Trans. Geosci. Remote Sens.*, 24, 906–919.

Prince, S.D., Kerr, Y.H., Goutorbe, J.P., Lebel, T., Tinga, A., Bessemoulin, P., Brouwer, J., Dolman, A.J., Engman, E.T., Gash, J.C.H., Hoepffner, M., Kabat, P., Monteny, B., Said, F., Sellers, P. and Wallace, J., 1995. Geographical, Biological and Remote Sensing aspects of the Hydrologic Atmospheric Pilot Experiment in the Sahel (HAPEX-Sahel). *Remote Sens. Environ.*, 51, 215–234.

Ross, J., 1981. *The Radiation Regime and Architecture of Plant Stands*. Junk. The Hague, 391 pp.

Roujean, J-L., Leroy, M. and Deschamps, P.Y., 1992. A bidirectional reflectance model of the earth's surface for the correction of remote sensing data. *J. Geophys. Res.* 97, 20455–20468.

Running, S.W., Justice, C.O., Salomonson, V., Hall, D., Barker, J., Kaufman, Y.J., Strahler, A.H., Huete, A.R., Muller, J.-P., Vanderbilt, V., Wan, Z.M., Teillet, P. and Carneggie, D. 1994. Terrestrial remote sensing science and algorithm planned for EOS/MODIS, *Int. J. Remote Sens.*, 15, 3587–3620.

van Leeuwen, W., Huete, A., Didan, K. and Liang, T., 1997. Modelling bi-directional reflectance factors for different land cover types and surface components to standardise vegetation indices. In: *Proceedings of the 7th International Symposium on Physical Measurements and Spectral Signatures in Remote Sensing* Courchevel, France. ISPRS Commission VII Vol. 1. 373–380.

Vermote, E.F., Tanré, D., Deuzé, J.L., Herman, M. and Morcrette, J.J., 1997. Second Simulation of the Satellite Signal in the Solar Spectrum: an overview, IEEE *Trans. Geosci. Remote Sens.*, 35, 5.

Wanner, W., Li, X. and Strahler, A., 1995. On the derivation of kernels for kernel-driven models of bidirectional reflectance, *J. Geophys. Res.*, 100, 21077–21089;

Wanner, W., Lewis, P. and Roujean, J-L., 1996. The influence of directional sampling on bidirectional reflectance and albedo